Analytical Solution of the Peridynamic Equation of Motion for a 2-Dimensional Rectangular Membrane

Zhenghao Yang[1,*], Chien-Ching Ma[1], Erkan Oterkus[2], Selda Oterkus[2], Konstantin Naumenko[3], Bozo Vazic[4]

[1]Department of Mechanical Engineering, National Taiwan University, Taipei, Taiwan

[2]PeriDynamics Research Centre, Department of Naval Architecture, Ocean and Marine Engineering, University of Strathclyde, Glasgow, United Kingdom

[3]Otto von Guericke University, Institute of Mechanics, Magdeburg, Germany

[4]Department of Mechanical Engineering, University of Utah, Salt Lake City, USA

Abstract

In order to analyse the deformation response of materials and structures, various continuum mechanics theories have been proposed. Peridynamics is a new non-local continuum mechanics formulation which has governing equations in integro-differential equation form. Analytical solution of these integro-differential equations is limited in the literature. In this study, analytical solution of the peridynamic equation of motion for a 2-dimensional membrane is presented. Analytical solutions are obtained for both static and dynamic conditions. Various numerical cases are considered to validate the derived analytical solution by comparing peridynamic results against classical continuum mechanics results. For both static and dynamic cases, both solutions agree very well with each other. Moreover, the influence of the size of the length scale parameter in peridynamics, horizon, is investigated. According to the numerical results, it is concluded that as the horizon size becomes larger, peridynamic solution captures nonlocal characteristics and peridynamic results deviate from classical continuum mechanics results.

Keywords: peridynamics; non-local; analytical; two-dimensional; membrane

1. Introduction

In order to analyse the deformation response of materials and structures, various continuum mechanics formulations have been proposed such as classical continuum mechanics (CCM), strain gradient elasticity, etc. CCM has been successfully utilised for the solution of many challenging problems. However, it also has certain limitations especially due to the type of equations that it is based on, i.e. partial differential equations. Since spatial derivatives do not exist along crack surfaces, governing equations of CCM cannot be directly utilised for the analysis of problems including discontinuities in the displacement field which mainly occurs in fracture problems. To overcome this limitation, a new nonlocal continuum mechanics approach, peridynamics (PD) [1, 2] was introduced without using spatial derivatives in the formulation and having integro-differential equations as the governing equation. Due to its nonlocal characteristic, it also has a length scale parameter named as horizon. PD is fundamentally different than some other approaches such as Smoothed Particle (SPH) Hydrodynamics and Element-free Galerkin approach (EFG). As opposed to peridynamics, SPH is based on curve fitting to approximate spatial derivatives of partial differential equations [3] and EFG is utilised for solving partial differential equations with moving least squares interpolants [4].

Since the introduction of peridynamics in 2000, there has been a significant progress in PD research and quite a large number of papers have been published especially during the last few years. Amongst these, Wu and Ren [5] utilised peridynamics for failure analysis of metal machining process. Diyaroglu et. al. [6] investigated the response of composite structures subjected to extreme loading by using peridynamics. Sun and Huang [7] performed peridynamic simulations to model impact damage in composite structures. In another study, Oterkus et. al. [8] used peridynamics for the investigation of impact damage in reinforced concrete. Gerstle et.

*Corresponding author: yangzh2006@hotmail.com

al. [9] also used peridynamics for modelling concrete material. Fracture analysis of functionally graded materials was explored by using peridynamics in Ozdemir et. al. [10] and Cheng et. al. [11]. Liu et. al. [12] utilised peridynamics for fracture analysis of graphene sheets whereas Silling et. al. [13] developed a peridynamic model for single-layer graphene based on coarse-grained bond forces. Ice fracture was also analysed in different studies such as Vazic et. al. [14] and Liu et. al. [15]. Madenci and Oterkus [16] presented how plasticity can be incorporated in peridynamic framework. Moreover, Huang et. al. [17] and Amani et. al. [18] provided peridynamic formulations suitable for viscoelastic and viscoplastic analyses. Various peridynamic beam and plate formulations have also been proposed such as refined zigzag beam and plate formulations by Dorduncu [19, 20], higher order beam and Kirchoff plate formulations by Yang et. al. [21, 22]. In addition, Naumenko and Eremeyev [23] presented a non-linear direct peridynamics plate theory and Chowdhury et. al. [24] developed a linear elastic peridynamic shell formulation. Peridynamics has also been used for predicting fatigue damage as presented in Nguyen et. al. [25] and Jung and Seok [26]. Kefal et. al. [27] and Heo et. al. [28] performed topology optimisation analysis and buckling analysis of cracked structures, respectively. Vazic et. al. [29] utilised peridynamics for the analysis of macrocrack and microcrack interactions. On the other hand, Imachi et. al. [30] performed dynamic crack arrest analysis by using peridynamics. Peridynamics has also been used in analysing other physical fields such as moisture diffusion as in Diyaroglu et. al. [31]. Corrosion damage and pit-to-crack phenomenon were also simulated within peridynamic framework by Shi et. al. [32] and De Meo et. al. [33], respectively.

In addition to these studies, there are also various studies in the literature focusing on peridynamic analysis of membranes. For example, Silling and Bobaru [34] utilised a constitutive model suitable for rubbery sheets that can form cracks to perform simulations of stretching and dynamic tearing of membranes. Oterkus et. al. [35] introduced a new peridynamic shell membrane formulation by using Euler-Lagrange equations. Li et. al. [36] used an implicit bond-based peridynamic formulation to analyse quasi-static large deformation, wrinkling and fracture of membranes. Bang and Madenci [37] developed peridynamic strain energy functions for a Non-Hookean type membrane under equibiaxial, planar, and uniaxial loading conditions. Madenci et. al. [38] presented a new approach to investigate the effect of membrane-inclusion interactions of different geometries with curvature, boundary conditions, and the contact angle between the membrane and inclusion. Ozdemir et. al. [39] proposed a viscoelastic material model in the ordinary-state based peridynamic framework to examine the crack propagation in polymeric water treatment membranes. Taylor et. al. [40] simulated the formation of spontaneous ruptures in supported phospholipid double bilayer membranes by using peridynamics.

Peridynamic equations are generally solved by using numerical techniques such as meshless approach. Although limited, analytical solutions are also available. For instance, Silling et. al. [41] provided an analytical solution for an infinite bar subjected to a self-equilibrated load distribution whereas Weckner and Abeyaratne [42] presented an analytical solution for an infinite bar by considering the effects of long-range forces. In another study, Weckner et. al. [43] derived peridynamic equations utilising Green's functions, Laplace and Fourier transforms for three-dimensional problems. Analytical solution for a 1-Dimensional rod was provided by Mikata [44]. More recently, Mikata [45] derived peridynamic solution for the analysis acoustic problems. An extensive review about peridynamic research is given in Javili et. al. [46].

As opposed to these aforementioned studies, this study presents analytical solution of the peridynamic equation of motion for 2-Dimensional membranes for the first time in the literature. Both static and dynamic conditions are considered. Anaytical solutions are provided for different initial conditions and peridynamic results are compared against results obtained from CCM for validation purposes. The influence of horizon size is also investigated.

2. Analytical Solution for a 2-Dimensional Membrane: Static Condition

Equilibrium equation for 2-Dimesional membranes can be expressed in CCM as:

$$k^2\left(\frac{\partial^2 w}{\partial x^2}+\frac{\partial^2 w}{\partial y^2}\right)+p(x,y)=0 \tag{1}$$

where k^2 denotes the material property parameter of the membrane, w is the deflection and p is the distributed transverse load. In PD theory, the corresponding formulation can be expressed as

$$\begin{aligned} &c\int_0^{2\pi}\int_0^{\delta}\frac{w(x+\xi_1,y+\xi_2)-w(x,y)}{\xi}\xi d\xi d\varphi+p(x,y)=0 \\ &c=\frac{6k^2}{\pi\delta^3}\quad \xi_1=\xi\cos\varphi\quad \xi_2=\xi\sin\varphi \end{aligned} \tag{2}$$

where the integral domain is chosen as the horizon of $\mathbf{x}$, $H_{\boldsymbol{x}}=B(\mathbf{x},\delta)$, and c is the bond constant, δ is the horizon size, ξ and φ represent the distance and angle between the material point of interest and its family member in the horizon (see Fig. 1). The derivation of Eq. (2) is given in Appendix.

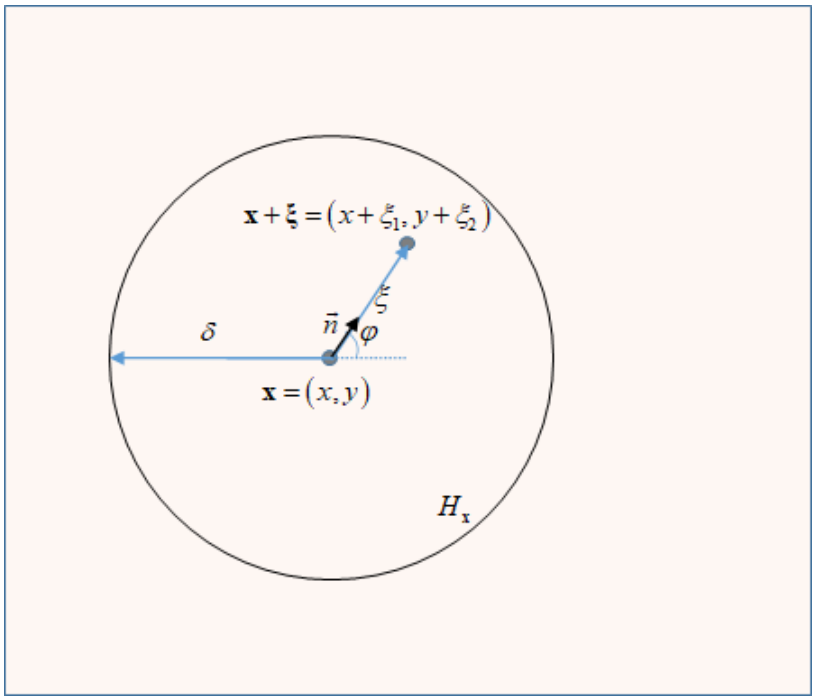

Figure 1. The distance and angle between the material point of interest and its family member.

Suppose that the rectangular domain is subjected to a distributed load of $p(x,y)$ (see Fig. 2) and the boundary condition is specified as

$$\text{BCs: }\begin{cases} w(0,y)=0 \\ w(a,y)=0 \\ w(x,0)=0 \\ w(x,b)=0 \end{cases} \tag{3}$$

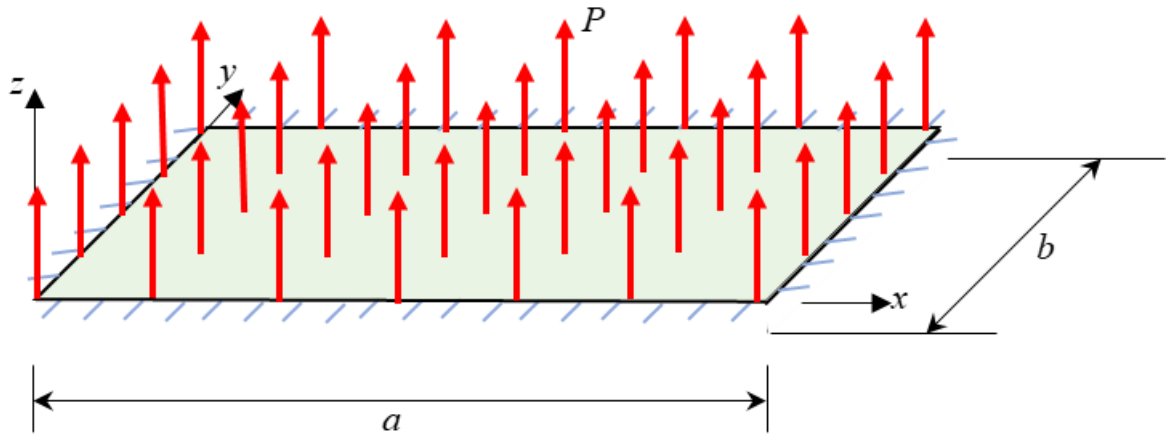

Figure 2. The rectangular domain subjected to a distributed load of $p(x,y)$.

Applying the boundary conditions to the CCM governing equations implies

$$\begin{cases} \left.\dfrac{\partial^2 w(x,y)}{\partial x^2}\right|_{x=0} = 0 \quad ; \quad \left.\dfrac{\partial^2 w(x,y)}{\partial x^2}\right|_{x=a} = 0 \\ \left.\dfrac{\partial^2 w(x,y)}{\partial y^2}\right|_{y=0} = 0 \quad ; \quad \left.\dfrac{\partial^2 w(x,y)}{\partial y^2}\right|_{y=b} = 0 \end{cases} \tag{4}$$

Performing central difference for Eq. (4) results in

$$\begin{cases} \dfrac{w(-h,y)-2w(0,y)+w(h,y)}{h^2} = 0 \quad ; \quad \dfrac{w(a-h,y)-2w(a,y)+w(a+h,y)}{h^2} = 0 \\ \dfrac{w(x,-h)-2w(x,0)+w(x,h)}{h^2} = 0 \quad ; \quad \dfrac{w(x,b-h)-2w(x,b)+w(x,b+h)}{h^2} = 0 \end{cases} \tag{5}$$

Replacing h by PD notation parameter ξ in Eq. (5), boundary conditions given in Eq. (3) yields the corresponding boundary conditions in PD theory as:

$$\text{PD BCs: } \begin{cases} w(-\xi,y) = -w(\xi,y) \quad ; \quad w(a-\xi,y) = -w(a+\xi,y) \\ w(x,-\xi) = -w(x,\xi) \quad ; \quad w(x,b-\xi) = -w(x,b+\xi) \end{cases} \tag{6}$$

To ensure that PD boundary conditions given in Eq. (6) are satisfied, we can assume the displacement field in the form of

$$w(x,y) = \sum_{n=1}^{\infty}\sum_{m=1}^{\infty} B_{nm} \sin\frac{m\pi x}{a}\sin\frac{n\pi y}{b} \tag{7}$$

Substituting Eq. (7) into the PD governing equation given in Eq. (2) gives

$$c\sum_{m=1}^{\infty}\sum_{n=1}^{\infty} B_{mn}\int_0^{2\pi}\int_0^{\delta}\frac{1}{\xi}\left[\sin\frac{m\pi(x+\xi_1)}{a}\sin\frac{n\pi(y+\xi_2)}{b} - \sin\frac{m\pi x}{a}\sin\frac{n\pi y}{b}\right]\xi d\xi d\varphi + p(x,y) = 0 \tag{8}$$

which can be simplified as

$$c\sum_{m=1}^{\infty}\sum_{n=1}^{\infty} B_{mn}\int_0^{2\pi}\int_0^{\delta}\frac{1}{\xi}\left(\cos\frac{m\pi\xi_1}{a}\cos\frac{n\pi\xi_2}{b} - 1\right)\xi d\xi d\varphi \sin\frac{m\pi x}{a}\sin\frac{n\pi y}{b} = -p(x,y) \tag{9}$$

The coefficients in Eq. (9) can be determined as

$$B_{mn}=\frac{4}{ab}\frac{1}{c}\frac{\int_0^a\int_0^b p(x,y)\sin\frac{m\pi x}{a}\sin\frac{n\pi y}{b}dxdy}{\int_0^{2\pi}\int_0^{\delta}\frac{1}{\xi}\left(1-\cos\frac{m\pi\xi_1}{a}\cos\frac{n\pi\xi_2}{b}\right)\xi d\xi d\varphi} \tag{10}$$

Thus, by coupling Eq. (10) with (7), the PD analytical solution for the static condition can be written as

$$w(x,y)=\frac{4}{ab}\frac{1}{c}\sum_{n=1}^{\infty}\sum_{m=1}^{\infty}\frac{\int_0^a\int_0^b p(x,y)\sin\frac{m\pi x}{a}\sin\frac{n\pi y}{b}dxdy}{\int_0^{2\pi}\int_0^{\delta}\frac{1}{\xi}\left(1-\cos\frac{m\pi\xi_1}{a}\cos\frac{n\pi\xi_2}{b}\right)\xi d\xi d\varphi}\sin\frac{m\pi x}{a}\sin\frac{n\pi y}{b} \tag{11}$$

The detailed derivation of the parameter B_{mn} is given in Appendix.

3. Analytical Solution for a 2-Dimensional Membrane: Dynamic Condition

PD governing equation given in Eq. (2) for static conditions can be extended to free vibrational conditions as:

$$\ddot{w}(x,y,t)=c\int_0^{2\pi}\int_0^{\delta}\frac{w(x+\xi_1,y+\xi_2,t)-w(x,y,t)}{\xi}\xi d\xi d\varphi \tag{12}$$

where $\ddot{w}(x,y,t)$ is the second derivative of the displacement $w(x,y,t)$ with respect to time, *t*. By utilising separation of variables approach, the displacement $w(x,y,t)$ can be written as:

$$w(x,y,t)=W(x,y)T(t) \tag{13}$$

Boundary conditions (BCs) and initial conditions (ICs) can be specified as:

$$\text{BCs: }\begin{cases} w(-\xi,y,t)=-w(\xi,y,t) \\ w(a-\xi,y,t)=-w(a+\xi,y,t) \\ w(x,-\xi,t)=-w(x,\xi,t) \\ w(x,b-\xi,t)=-w(x,b+\xi,t) \end{cases}\Rightarrow\begin{cases} W(-\xi,y)=-W(\xi,y) \\ W(a-\xi,y)=-W(a+\xi,y) \\ W(x,-\xi)=-W(x,\xi) \\ W(x,b-\xi)=-W(x,b+\xi) \end{cases} \tag{14}$$

$$\text{ICs: }\begin{cases} w(x,y,0)=w_0(x,y) \\ \dot{w}(x,y,0)=v_0(x,y) \end{cases} \tag{15}$$

where $\dot{w}$ is the first derivative of the displacement $w(x,y,t)$ with respect to time. By substituting Eq. (13) in Eq. (12) yields:

$$W(x,y)\ddot{T}(t)=cT(t)\int_0^{2\pi}\int_0^{\delta}\frac{W(x+\xi_1,y+\xi_2)-W(x,y)}{\xi}\xi d\xi d\varphi \tag{16}$$

Rearranging Eq. (16) results in:

$$\frac{1}{c}\frac{\ddot{T}(t)}{T(t)}=\frac{1}{W(x,y)}\int_0^{2\pi}\int_0^{\delta}\frac{W(x+\xi_1,y+\xi_2)-W(x,y)}{\xi}\xi d\xi d\varphi=-\lambda \tag{17}$$

which gives two separate equations:

$$\int_0^{2\pi}\int_0^{\delta}\frac{W\left(x+\xi_1,y+\xi_2\right)-W\left(x,y\right)}{\xi}\xi d\xi d\varphi=-\lambda W\left(x,y\right) \tag{18a}$$

and

$$\ddot{T}\left(t\right)+c\lambda T\left(t\right)=0 \tag{18b}$$

Comparing Eq. (18a) to (2) and if we consider $W(x,y)$ as an analogue to $w(x,y)$ and $-\lambda W(x,y)$ as to $p(x,y)/c$, the following equation can be obtained by utilizing Eq. (7) and (9) as

$$\sum_{m=1}^{\infty}\sum_{n=1}^{\infty}B_{mn}^{*}\int_0^{2\pi}\int_0^{\delta}\frac{1}{\xi}\left(\cos\frac{m\pi\xi_1}{a}\cos\frac{n\pi\xi_2}{b}-1\right)\xi d\xi d\varphi\sin\frac{m\pi x}{a}\sin\frac{n\pi y}{b}=-\sum_{m=1}^{\infty}\sum_{n=1}^{\infty}\lambda_{mn}B_{mn}^{*}\sin\frac{m\pi x}{a}\sin\frac{n\pi y}{b} \tag{19}$$

In Eq. (19), the ‘’pseudo eigenvalue’’ can be defined as

$$\lambda_{mn}=\int_0^{2\pi}\int_0^{\delta}\frac{1}{\xi}\left(1-\cos\frac{m\pi\xi_1}{a}\cos\frac{n\pi\xi_2}{b}\right)\xi d\xi d\varphi \tag{20}$$

Next, the general solution to Eq. (18b) can be given as

$$T_{mn}\left(t\right)=A_{mn}\cos\left(\sqrt{\lambda_{mn}}ct\right)+B_{mn}\sin\left(\sqrt{\lambda_{mn}}ct\right) \tag{21}$$

Finally, according to superposition principle, the general solution to Eq. (13) can be written as the linear combination of each mode as

$$w\left(x,y,t\right)=\sum_{m=1}^{\infty}\sum_{n=1}^{\infty}\left[A_{mn}\cos\left(\sqrt{\lambda_{mn}}ct\right)+B_{mn}\sin\left(\sqrt{\lambda_{mn}}ct\right)\right]\sin\frac{m\pi x}{a}\sin\frac{n\pi y}{b} \tag{22}$$

Since dynamic condition is considered, initial conditions can be written as:

$$w_0\left(x,y\right)=\sum_{m=1}^{\infty}\sum_{n=1}^{\infty}A_{mn}\sin\frac{m\pi x}{a}\sin\frac{n\pi y}{b} \tag{23a}$$

and

$$v_0\left(x,y\right)=\sum_{m=1}^{\infty}\sum_{n=1}^{\infty}B_{mn}\sqrt{\lambda_{mn}}c\sin\frac{m\pi x}{a}\sin\frac{n\pi y}{b} \tag{23b}$$

in which the coefficients can be calculated based on orthogonal property as

$$A_{mn}=\frac{4}{ab}\int_0^{b}\int_0^{a}w_0\left(x,y\right)\sin\frac{m\pi x}{a}\sin\frac{n\pi y}{b}dxdy \tag{24a}$$

$$B_{mn}=\frac{4}{ab}\frac{1}{\sqrt{\lambda_{mn}}c}\int_0^{b}\int_0^{a}v_0\left(x,y\right)\sin\frac{m\pi x}{a}\sin\frac{n\pi y}{b}dxdy \tag{24b}$$

By summarising the derivations above, the PD analytical solution for 2-D vibrational membrane can be written as

$$w\left(x,y,t\right)=\sum_{m=1}^{\infty}\sum_{n=1}^{\infty}\left[A_{mn}\cos\left(\sqrt{\lambda_{mn}}ct\right)+B_{mn}\sin\left(\sqrt{\lambda_{mn}}ct\right)\right]\sin\frac{m\pi x}{a}\sin\frac{n\pi y}{b} \tag{25a}$$

$$A_{mn} = \frac{4}{ab}\int_0^b \int_0^a w_0(x,y)\sin\frac{m\pi x}{a}\sin\frac{n\pi y}{b}dxdy \tag{25b}$$

$$B_{mn} = \frac{4}{ab}\frac{1}{\sqrt{\lambda_{mn}c}}\int_0^b \int_0^a v_0(x,y)\sin\frac{m\pi x}{a}\sin\frac{n\pi y}{b}dxdy \tag{25c}$$

$$\lambda_{mn} = \int_0^{2\pi}\int_0^{\delta}\frac{1}{\xi}\left(1-\cos\frac{m\pi\xi_1}{a}\cos\frac{n\pi\xi_2}{b}\right)\xi d\xi d\varphi \tag{25d}$$

$$c = \frac{6k^2}{\pi\delta^3} \quad \xi_1 = \xi\cos\varphi \quad \xi_2 = \xi\sin\varphi \tag{25e}$$

4. Numerical Results

4.1. 2-Dimensional membrane under static condition

In the first case, a 2-Dimensional membrane with all edges fixed subjected to a distributed load under static condition is considered. The dimensions of the membrane are specified as a=b=1m. The material parameter k^2 is 1e5 Nm/kg. The horizon size is chosen as δ = 0.001 m. The distributed load is exerted as $p(x) = -xy(x-a)(y-b)$.

The variation of the displacement w along central x-axis and central y-axis obtained by using PD and CCM are shown in Fig. 3. According to these results, it can be observed that a very good agreement is obtained between the two solutions.

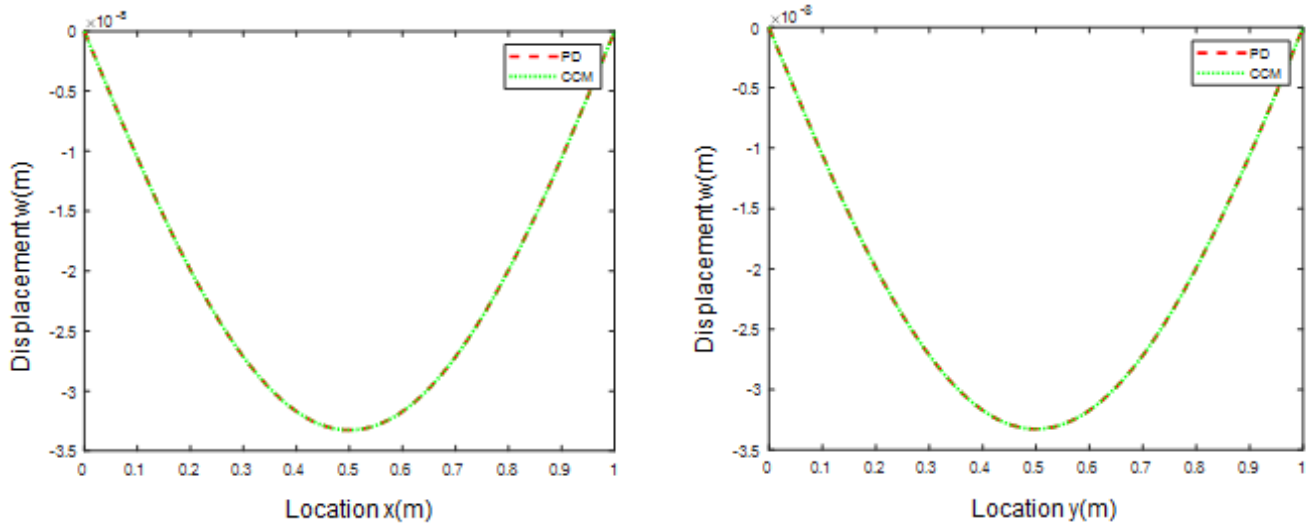

(a) **(b)**

Figure 3. Variation of the displacement w along **(a)** central x-axis and **(b)** central y-axis.

The variation of the displacement w along the 2-Dimensional membrane is also demonstrated in Fig. 4. As can be seen in this figure, PD and CCM results agree very well with each other.

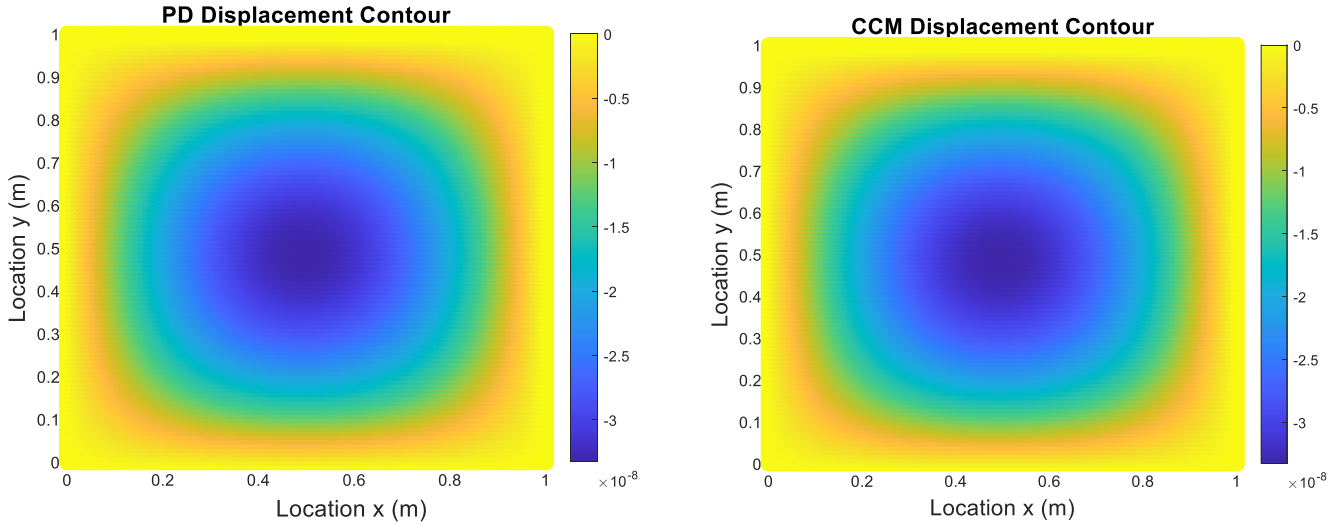

(a) **(b)**

Figure 4. Variation of the displacement w along the 2-Dimensional membrane **(a)** PD results and **(b)** CCM results.

4.2. 2-Dimensional membrane under dynamic condition

In the second example case, the numerical case considered in the previous case is extended for a dynamic condition. The distributed load is removed and the initial condition is imposed as:

$$\text{ICs: } \begin{cases} w_0(x,y) = 0.001xy(x-1)(y-1) \\ v_0(x,y) = 0 \end{cases} \tag{26}$$

Variation of the displacement w at x = 0.5m and y = 0.5m as the time progresses is shown in Fig. 5. A very good agreement is observed between PD and CCM solutions at all times.

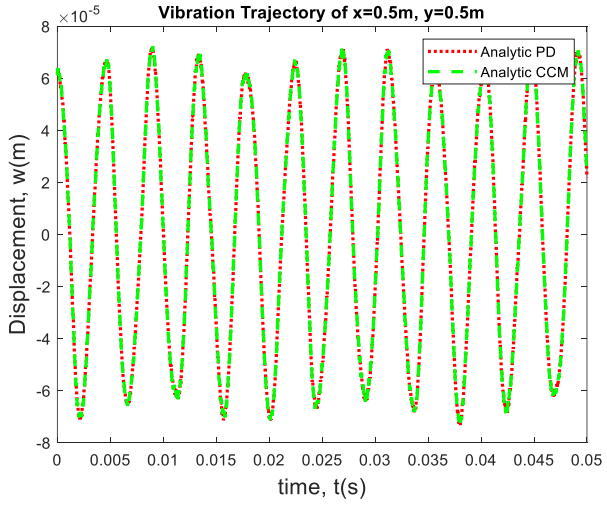

Figure 5. Variation of the displacement w at x = 0.5m and y = 0.5m as the time progresses.

4.3. 2-Dimensional membrane under dynamic condition with different initial conditions

In the third case, the initial case considered in the previous case is replaced by

$$\text{ICs: } \begin{cases} w_0(x,y) = 0.01xy(x-1)(y-1) \\ v_0(x,y) = 100xy(x-1)(y-1) \end{cases} \tag{27}$$

The variation of the displacement w at three different locations, x = 0.5m and y = 1m, x = 0.25m and y = 1m, and x = 0.25m and y = 0.5m as the time progresses is demonstrated in Figs. 6-8. At all three locations, PD results agree very well with CCM results.

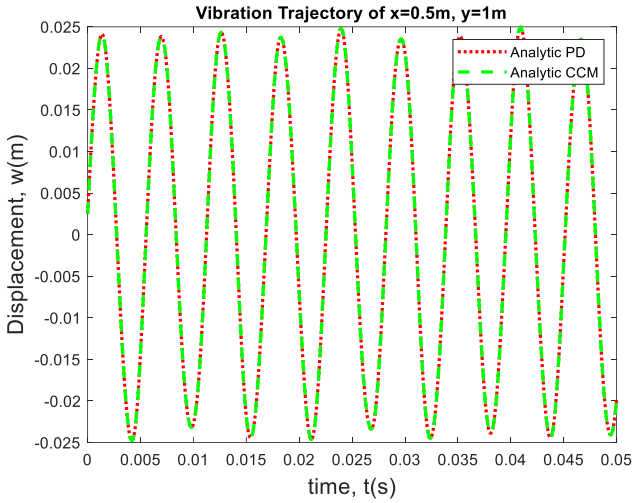

Figure 6. Variation of the displacement w at x = 0.5m and y = 1m as the time progresses.

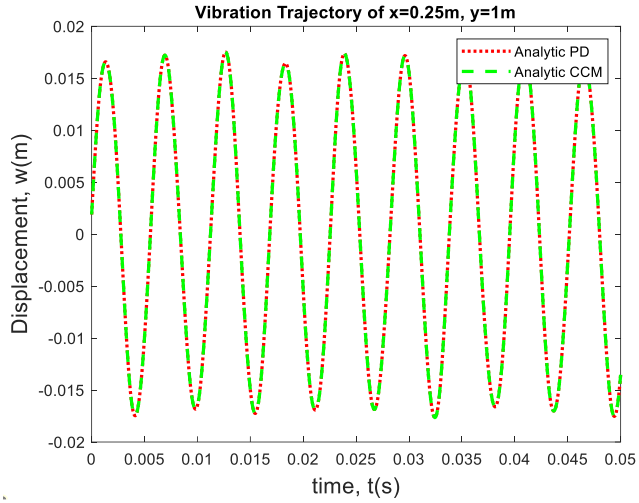

Figure 7. Variation of the displacement w at x = 0.25m and y = 1m as the time progresses.

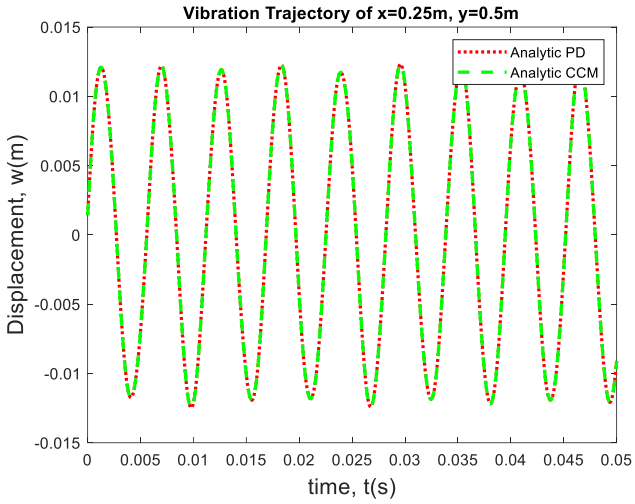

Figure 8. Variation of the displacement w at $x = 0.25$m and $y = 0.5$m as the time progresses.

4.4. Effect of variation of horizon size

In the final numerical case, the influence of the horizon size on the results is investigated by considering the horizon size as 0.005m, 0.01m, 0.05m and 0.1m. For this numerical case, the following initial conditions are considered as:

$$\text{ICs: } \begin{cases} u_0(x,y) = 0.01\left[xy(x-1)(y-1)\right]^2 \\ v_0(x,y) = 0 \end{cases} \tag{28}$$

Variation of the displacement w at two different locations, $x = 0.5$m and $y = 0.5$m, and $x = 0.25$m and $y = 0.25$m, as the time progresses for different horizon sizes are illustrated in Figs. 9-12. As shown in these figures, PD and CCM results match very well for the horizon size values of 0.005m and 0.01m. However, PD results deviate from CCM results for the horizon size values of 0.05m and 0.1m. This is expected since for large horizon sizes, nonlocal characteristic of PD starts to emerge and represent a behaviour different than classical (local) characteristic.

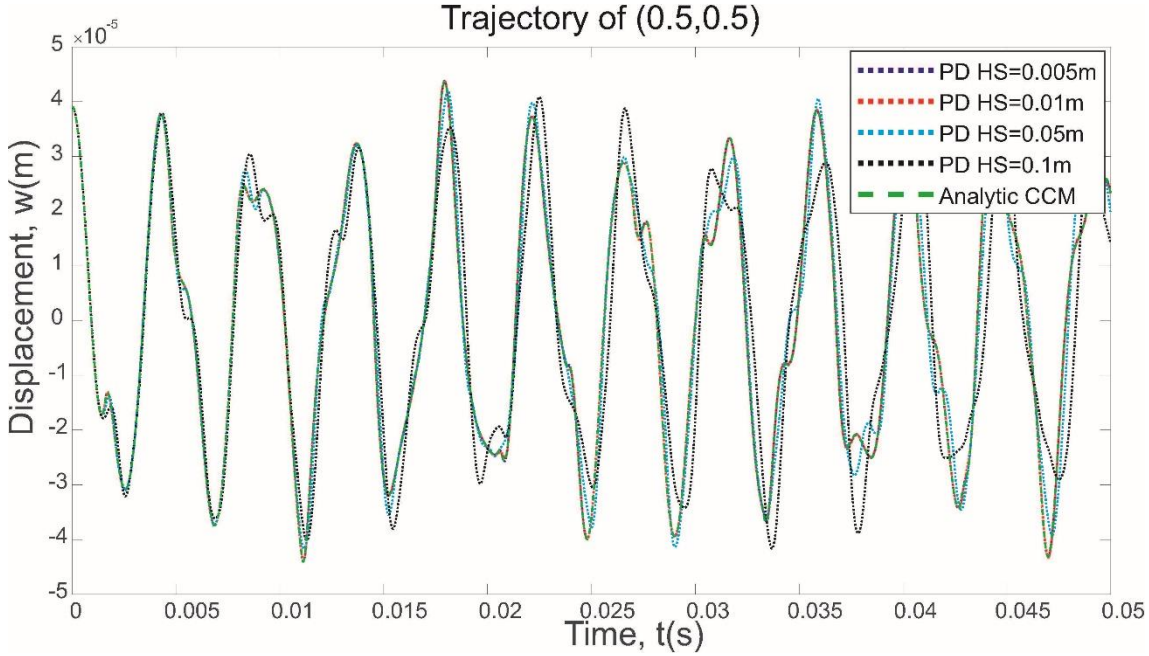

Figure 9. Variation of the displacement w at $x = 0.5$m and $y = 0.5$m as the time progresses for different horizon sizes.

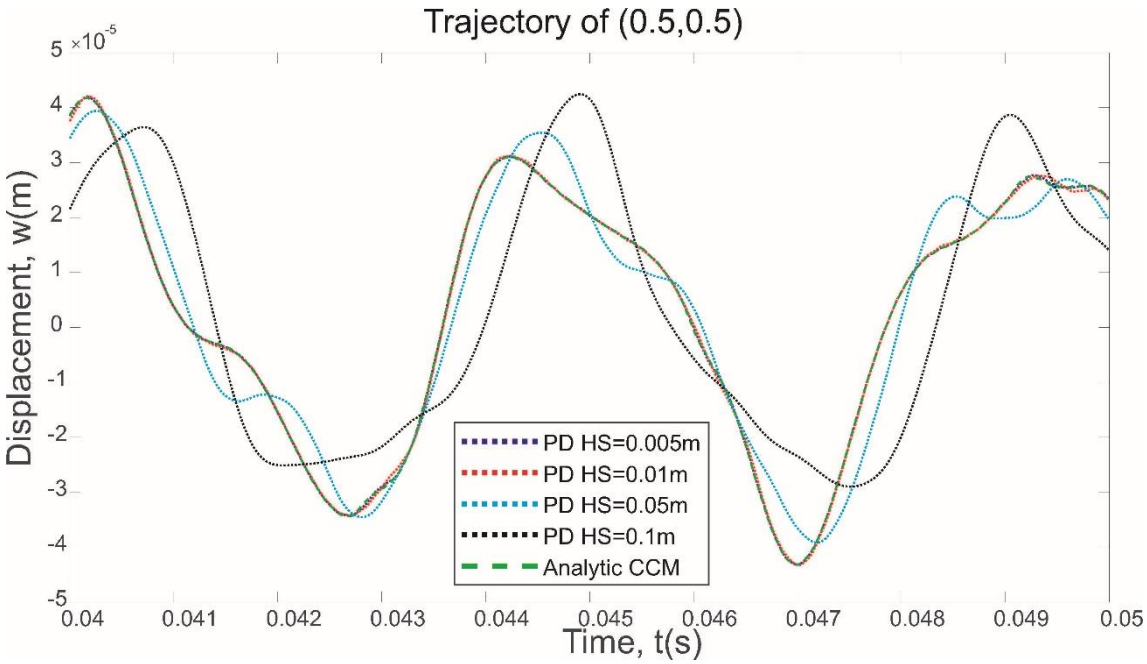

Figure 10. Variation of the displacement w at $x = 0.5$m and $y = 0.5$m as the time progresses for different horizon sizes (zoomed view).

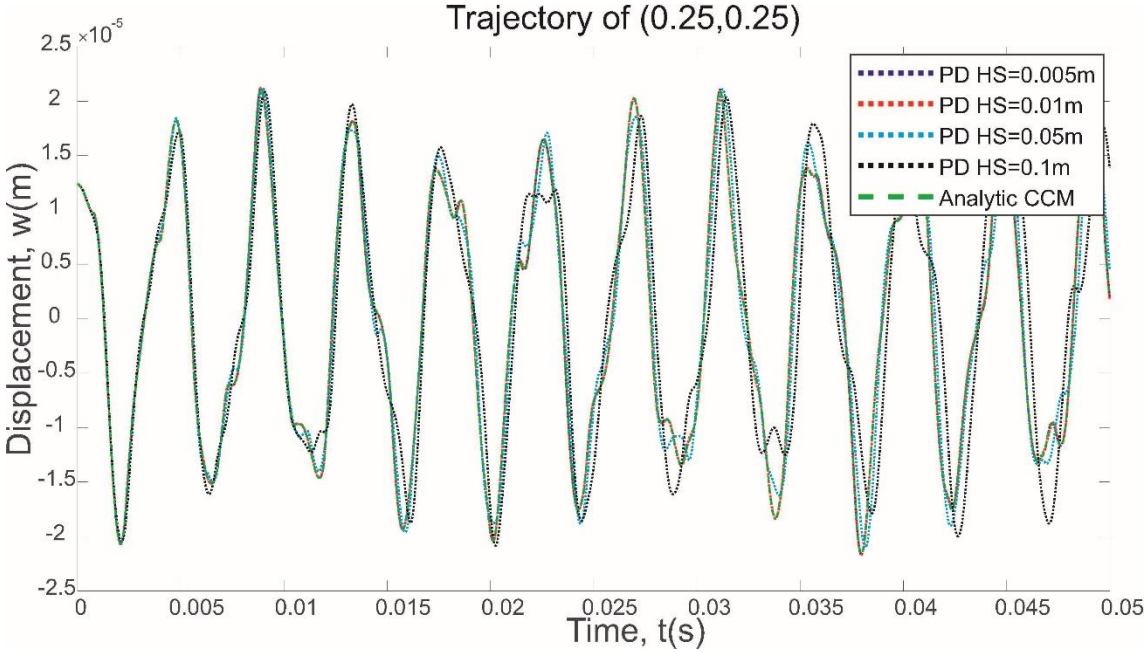

Figure 11. Variation of the displacement w at $x = 0.25$m and $y = 0.25$m as the time progresses for different horizon sizes.

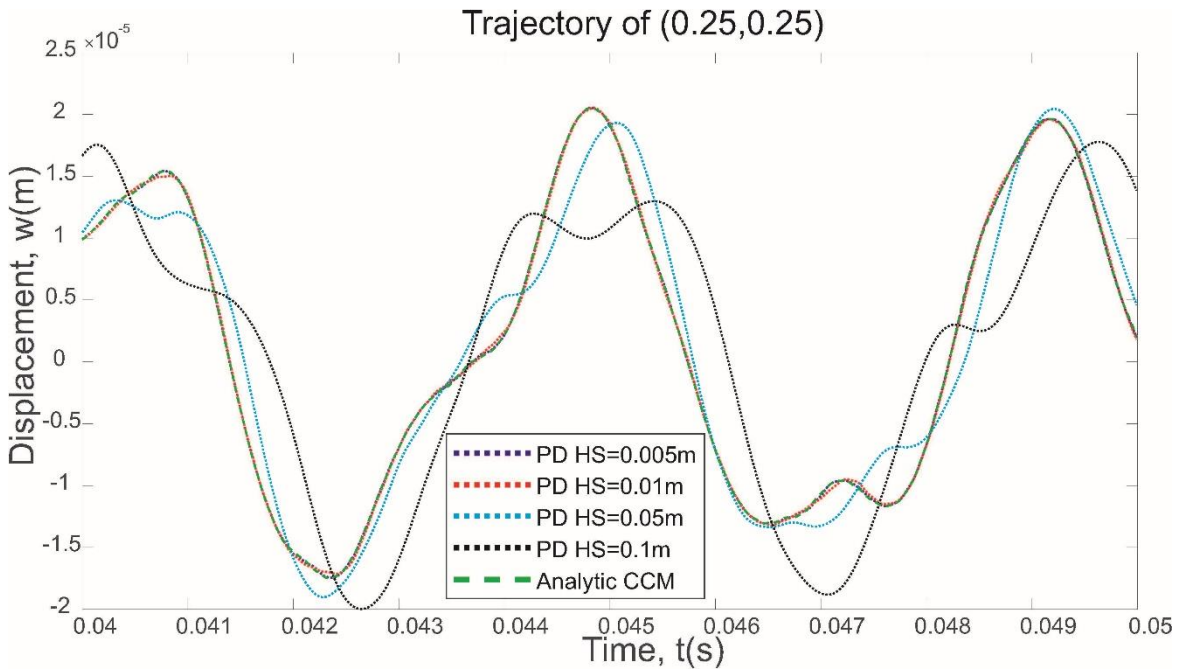

Figure 12. Variation of the displacement w at $x = 0.25$m and $y = 0.25$m as the time progresses for different horizon sizes (zoomed view).

5. Conclusions

In this study, analytical solution of the peridynamic equation of motion for a 2-dimensional membrane was presented. Several numerical cases were considered to validate the derived analytical approach. In the first case, a membrane subjected to distributed loading was analysed for static condition. Peridynamic results obtained along the central axes agree very well with the classical continuum mechanics results. In the second and third cases, dynamic conditions were considered by removing the distributed load and imposing two different initial conditions. Several points were selected and variation of peridynamic displacement results as the time progresses is compared with the classical continuum mechanics results. As in the static case, a very good agreement was obtained between peridynamic and classical continuum mechanics results. Finally, the influence of horizon size was investigated by considering four different horizon sizes. As the horizon sizes are getting bigger, it was observed that peridynamic results deviate from classical continuum mechanics results which show that peridynamics can represent nonlocal behaviour as the horizon size increases. The presented approach is not applicable for the cases with discontinuities such as cracks. Extension of the current approach to problems with discontinuities is a potential direction of future research.

Data Availability

The datasets generated during and/or analysed during the current study are available from the corresponding author on reasonable request.

References

[1] Silling, S.A., 2000. Reformulation of elasticity theory for discontinuities and long-range forces. *Journal of the Mechanics and Physics of Solids*, *48*(1), pp.175-209.

[2] Madenci, E. and Oterkus, E., 2014. *Peridynamic theory and its applications*. Springer, New York, NY.

[3] Silling, S.A., Demmie, P.N. and Warren, T.L., 2007. Peridynamic Simulation of High-Rate Material Failure (No. SAND2007-3464C). Sandia National Lab.(SNL-NM), Albuquerque, NM (United States).

[4] Lu, Y.Y., Belytschko, T. and Gu, L., 1994. A new implementation of the element free Galerkin method. Computer methods in applied mechanics and engineering, 113(3-4), pp.397-414.

[5] Wu, C.T. and Ren, B., 2015. A stabilized non-ordinary state-based peridynamics for the nonlocal ductile material failure analysis in metal machining process. *Computer Methods in Applied Mechanics and Engineering*, *291*, pp.197-215.

[6] Diyaroglu, C., Oterkus, E., Madenci, E., Rabczuk, T. and Siddiq, A., 2016. Peridynamic modeling of composite laminates under explosive loading. *Composite Structures*, *144*, pp.14-23.

[7] Sun, C. and Huang, Z., 2016. Peridynamic simulation to impacting damage in composite laminate. *Composite Structures*, *138*, pp.335-341.

[8] Oterkus, E., Guven, I. and Madenci, E., 2012. Impact damage assessment by using peridynamic theory. *Central European journal of engineering*, *2*(4), pp.523-531.

[9] Gerstle, W., Sau, N. and Silling, S., 2007. Peridynamic modeling of concrete structures. *Nuclear engineering and design*, *237*(12-13), pp.1250-1258.

[10] Ozdemir, M., Kefal, A., Imachi, M., Tanaka, S. and Oterkus, E., 2020. Dynamic fracture analysis of functionally graded materials using ordinary state-based peridynamics. *Composite Structures*, *244*, p.112296.

[11] Cheng, Z., Liu, Y., Zhao, J., Feng, H. and Wu, Y., 2018. Numerical simulation of crack propagation and branching in functionally graded materials using peridynamic modeling. *Engineering Fracture Mechanics*, *191*, pp.13-32.

[12] Liu, X., He, X., Wang, J., Sun, L. and Oterkus, E., 2018. An ordinary state-based peridynamic model for the fracture of zigzag graphene sheets. *Proceedings of the Royal Society A: Mathematical, Physical and Engineering Sciences*, *474*(2217), p.20180019.

[13] Silling, S.A., D'Elia, M., Yu, Y., You, H. and Fermen-Coker, M., 2022. Peridynamic Model for Single-Layer Graphene Obtained from Coarse-Grained Bond Forces. *Journal of Peridynamics and Nonlocal Modeling*, pp.1-22.

[14] Vazic, B., Oterkus, E. and Oterkus, S., 2020. Peridynamic model for a Mindlin plate resting on a Winkler elastic foundation. *Journal of Peridynamics and Nonlocal Modeling*, *2*(3), pp.229-242.

[15] Liu, R.W., Xue, Y.Z., Lu, X.K. and Cheng, W.X., 2018. Simulation of ship navigation in ice rubble based on peridynamics. *Ocean Engineering*, *148*, pp.286-298.

[16] Madenci, E. and Oterkus, S., 2016. Ordinary state-based peridynamics for plastic deformation according to von Mises yield criteria with isotropic hardening. *Journal of the Mechanics and Physics of Solids*, *86*, pp.192-219.

[17] Huang, Y., Oterkus, S., Hou, H., Oterkus, E., Wei, Z. and Zhang, S., 2019. Peridynamic model for visco-hyperelastic material deformation in different strain rates. *Continuum Mechanics and Thermodynamics*, pp.1-35.

[18] Amani, J., Oterkus, E., Areias, P., Zi, G., Nguyen-Thoi, T. and Rabczuk, T., 2016. A non-ordinary state-based peridynamics formulation for thermoplastic fracture. *International Journal of Impact Engineering*, *87*, pp.83-94.

[19] Dorduncu, M., 2019. Stress analysis of laminated composite beams using refined zigzag theory and peridynamic differential operator. *Composite Structures*, *218*, pp.193-203.

[20] Dorduncu, M., 2020. Stress analysis of sandwich plates with functionally graded cores using peridynamic differential operator and refined zigzag theory. *Thin-Walled Structures*, *146*, p.106468.

[21] Yang, Z., Oterkus, E. and Oterkus, S., 2021. Peridynamic higher-order beam formulation. *Journal of Peridynamics and Nonlocal Modeling*, *3*(1), pp.67-83.

[22] Yang, Z., Vazic, B., Diyaroglu, C., Oterkus, E. and Oterkus, S., 2020. A Kirchhoff plate formulation in a state-based peridynamic framework. *Mathematics and Mechanics of Solids*, *25*(3), pp.727-738.

[23] Naumenko, K. and Eremeyev, V.A., 2022. A non-linear direct peridynamics plate theory. *Composite Structures*, *279*, p.114728.

[24] Chowdhury, S.R., Roy, P., Roy, D. and Reddy, J.N., 2016. A peridynamic theory for linear elastic shells. *International Journal of Solids and Structures*, *84*, pp.110-132.

[25] Nguyen, C.T., Oterkus, S. and Oterkus, E., 2021. An energy-based peridynamic model for fatigue cracking. *Engineering Fracture Mechanics*, *241*, p.107373.

[26] Jung, J. and Seok, J., 2017. Mixed-mode fatigue crack growth analysis using peridynamic approach. *International Journal of Fatigue*, *103*, pp.591-603.

[27] Kefal, A., Sohouli, A., Oterkus, E., Yildiz, M. and Suleman, A., 2019. Topology optimization of cracked structures using peridynamics. *Continuum Mechanics and Thermodynamics*, *31*(6), pp.1645-1672.

[28] Heo, J., Yang, Z., Xia, W., Oterkus, S. and Oterkus, E., 2020. Buckling analysis of cracked plates using peridynamics. *Ocean Engineering*, *214*, p.107817.

[29] Vazic, B., Wang, H., Diyaroglu, C., Oterkus, S. and Oterkus, E., 2017. Dynamic propagation of a macrocrack interacting with parallel small cracks. *AIMS Materials Science*, *4*(1), pp.118-136.

[30] Imachi, M., Tanaka, S., Ozdemir, M., Bui, T.Q., Oterkus, S. and Oterkus, E., 2020. Dynamic crack arrest analysis by ordinary state-based peridynamics. *International Journal of Fracture*, *221*(2), pp.155-169.

[31] Diyaroglu, C., Oterkus, S., Oterkus, E., Madenci, E., Han, S. and Hwang, Y., 2017. Peridynamic wetness approach for moisture concentration analysis in electronic packages. *Microelectronics Reliability*, *70*, pp.103-111.

[32] Shi, C., Gong, Y., Yang, Z.G. and Tong, Q., 2019. Peridynamic investigation of stress corrosion cracking in carbon steel pipes. *Engineering Fracture Mechanics*, *219*, p.106604.

[33] De Meo, D., Russo, L. and Oterkus, E., 2017. Modeling of the onset, propagation, and interaction of multiple cracks generated from corrosion pits by using peridynamics. *Journal of Engineering Materials and Technology*, *139*(4), p.041001.

[34] Silling, S.A. and Bobaru, F., 2005. Peridynamic modeling of membranes and fibers. *International Journal of Non-Linear Mechanics*, *40*(2-3), pp.395-409.

[35] Oterkus, E., Madenci, E. and Oterkus, S., 2020. Peridynamic shell membrane formulation. *Procedia Structural Integrity*, *28*, pp.411-417.

[36] Li, H., Zheng, Y.G., Zhang, Y.X., Ye, H.F. and Zhang, H.W., 2019. Large deformation and wrinkling analyses of bimodular structures and membranes based on a peridynamic computational framework. *Acta Mechanica Sinica*, *35*(6), pp.1226-1240.

[37] Bang, D.J. and Madenci, E., 2017. Peridynamic modeling of hyperelastic membrane deformation. *Journal of Engineering Materials and Technology*, *139*(3), p.031007.

[38] Madenci, E., Barut, A. and Purohit, P.K., 2020. A peridynamic approach to computation of elastic and entropic interactions of inclusions on a lipid membrane. *Journal of the Mechanics and Physics of Solids*, *143*, p.104046.

[39] Ozdemir, M., Oterkus, S., Oterkus, E., Amin, I., El-Aassar, A. and Shawky, H., 2022. Fracture simulation of viscoelastic membranes by ordinary state-based peridynamics. *Procedia Structural Integrity*, *41*, pp.333-342.

[40] Taylor, M., Gözen, I., Patel, S., Jesorka, A. and Bertoldi, K., 2016. Peridynamic modeling of ruptures in biomembranes. *PloS one*, *11*(11), p.e0165947.

[41] Silling, S.A., Zimmermann, M. and Abeyaratne, R., 2003. Deformation of a peridynamic bar. *Journal of Elasticity*, *73*(1), pp.173-190.

[42] Weckner, O. and Abeyaratne, R., 2005. The effect of long-range forces on the dynamics of a bar. *Journal of the Mechanics and Physics of Solids*, *53*(3), pp.705-728.

[43] Weckner, O., Brunk, G., Epton, M.A., Silling, S.A. and Askari, E., 2009. Green's functions in non-local three-dimensional linear elasticity. *Proceedings of the Royal Society A: Mathematical, Physical and Engineering Sciences*, *465*(2111), pp.3463-3487.

[44] Mikata, Y., 2012. Analytical solutions of peristatic and peridynamic problems for a 1D infinite rod. *International Journal of Solids and Structures*, *49*(21), pp.2887-2897.

[45] Mikata, Y., 2021. Peridynamics for fluid mechanics and acoustics. *Acta Mechanica*, *232*(8), pp.3011-3032.

[46] Javili, A., Morasata, R., Oterkus, E. and Oterkus, S., 2019. Peridynamics review. *Mathematics and Mechanics of Solids*, *24*(11), pp.3714-3739.

Appendix

Laplacian in 2D rectangular coordinate system can be written as

$$\Delta w = \frac{\partial^2 w}{\partial x_I \partial x_I} \tag{A1}$$

where the suffix takes up the value of 1 $(= x)$ and 2 $(= y)$. Performing Taylor expansion for w and omitting higher order terms yields

$$w\left(x+\xi_1, y+\xi_2\right) - w\left(x,y\right) = \left.\frac{\partial w}{\partial x_I}\right|_{(x,y)} \xi n_I + \frac{1}{2}\left.\frac{\partial^2 w}{\partial x_I \partial x_J}\right|_{(x,y)} \xi^2 n_I n_J \tag{A2}$$

in which $\boldsymbol{n}$ denotes the unit directional vector (see Fig. 1) such that

$$\begin{Bmatrix} n_1 \\ n_2 \end{Bmatrix} = \begin{Bmatrix} \cos\varphi \\ \sin\varphi \end{Bmatrix} \tag{A3}$$

Considering (x, y) as a fixed point, dividing each term in Eq. (A2) by ξ and integrating over its PD domain results in

$$\int_0^{2\pi}\int_0^{\delta} \frac{w\left(x+\xi_1, y+\xi_2\right) - w\left(x,y\right)}{\xi} \xi d\xi d\varphi = \left.\frac{\partial w}{\partial x_I}\right|_{(x,y)} \int_0^{2\pi}\int_0^{\delta} n_I \xi d\xi d\varphi + \frac{1}{2}\left.\frac{\partial^2 w}{\partial x_I \partial x_J}\right|_{(x,y)} \int_0^{2\pi}\int_0^{\delta} \xi n_I n_J \xi d\xi d\varphi \tag{A4}$$

which reduces to

$$\int_0^{2\pi}\int_0^{\delta} \frac{w\left(x+\xi_1, y+\xi_2\right) - w\left(x,y\right)}{\xi} \xi d\xi d\varphi = \frac{1}{2}\left.\frac{\partial^2 w}{\partial x_I \partial x_J}\right|_{(x,y)} \frac{\pi\delta^3}{3} \delta_{IJ} \tag{A5}$$

Finally, Eq. (A5) can be rewritten as

$$\left.\frac{\partial^2 w}{\partial x_I \partial x_I}\right|_{(x,y)} = \frac{6}{\pi\delta^3}\int_0^{2\pi}\int_0^{\delta}\frac{w(x+\xi_1, y+\xi_2)-w(x,y)}{\xi}\xi d\xi d\varphi \tag{A6}$$

Moreover, the parameter B_{mn} in Eq. (9) can be obtained by multiplying Eq. (9) by $\sin\frac{p\pi x}{a}\sin\frac{q\pi y}{b}$ and integrating over the domain of the body as

$$\begin{aligned} &c\sum_{m=1}^{\infty}\sum_{n=1}^{\infty}B_{mn}\int_0^{2\pi}\int_0^{\delta}\frac{1}{\xi}\left(\cos\frac{m\pi\xi_1}{a}\cos\frac{n\pi\xi_2}{b}-1\right)\xi d\xi d\varphi\int_0^a\int_0^b\sin\frac{m\pi x}{a}\sin\frac{n\pi y}{b}\sin\frac{p\pi x}{a}\sin\frac{q\pi y}{b}dxdy \\ &=-\int_0^a\int_0^b p(x,y)\sin\frac{p\pi x}{a}\sin\frac{q\pi y}{b}dxdy \end{aligned} \tag{A7}$$

According the orthogonality of trigonometric functions, i.e.

$$\int_0^a \sin\frac{m\pi x}{a}\sin\frac{p\pi x}{a}dx = \frac{a}{2}\delta_{pm} \qquad \text{and} \qquad \int_0^b \sin\frac{n\pi y}{b}\sin\frac{q\pi y}{b}dx = \frac{b}{2}\delta_{qn} \tag{A8}$$

Thus, Eq. (A7) becomes

$$cB_{pq}\int_0^{2\pi}\int_0^{\delta}\frac{1}{\xi}\left(\cos\frac{m\pi\xi_1}{a}\cos\frac{n\pi\xi_2}{b}-1\right)\xi d\xi d\varphi\frac{ab}{4} = -\int_0^a\int_0^b p(x,y)\sin\frac{p\pi x}{a}\sin\frac{q\pi y}{b}dxdy \tag{A9}$$

and the parameter B_{mn} can be obtained as:

$$B_{mn} = \frac{4}{ab}\frac{1}{c}\frac{\int_0^a\int_0^b p(x,y)\sin\frac{m\pi x}{a}\sin\frac{n\pi y}{b}dxdy}{\int_0^{2\pi}\int_0^{\delta}\frac{1}{\xi}\left(1-\cos\frac{m\pi\xi_1}{a}\cos\frac{n\pi\xi_2}{b}\right)\xi d\xi d\varphi} \tag{A10}$$